A Kinect-Based Approach for 3D Pavement Surface Reconstruction and Cracking Recognition

Yuming Zhang, Cong Chen, Qiong Wu, Qi Lu, Su Zhang, Guohui Zhang, *Member, IEEE*, and Yin Yang, *Member, IEEE*

***Abstract*— Pavement surface distress conditions are critical inputs for quantifying roadway infrastructure serviceability. Numerous computer-aided automatic examination techniques have been deployed for pavement distress condition assessments, such as digital image processing methods. However, their effectiveness and applicability are impeded due to information losses in 2-D image combination processes or extremely high costs in 3-D geo-referenced data set. In this paper, a cost-effective Kinect-based approach is proposed for 3-D pavement surface reconstruction and cracking recognition. We propose a comprehensive computational solution for the detection and recognition of pavement distress feature identification. Various cracking measurements such as alligator cracking, traverse cracking, longitudinal cracking, and so on. are identified and recognized for their severity examinations based on associated geometrical features. The experimental results indicate that this method is effective in reducing data collection costs and extracting analytical information on pavement cracking measurements. The research findings confirm that the proposed approach provides a viable, applicable solution to an automatic pavement surface condition detection and evaluation. The proposed methodology is transferable for pavement surface reconstruction and distress condition detection based on the other 3-D cloud point data. It provides an alternative inexpensive complement to existing pavement examination methodologies.**

***Index Terms*— Pavement distress severity, Kinect fusion, crack detection, pavement serviceability, surface reconstruction.**

I. Introduction

HIGH quality pavement serviceability is critical to maintain safe and effective traffic operations. As an indispensable component of the Pavement Management Systems (PMS), pavement condition evaluation is an essential procedure to provide comprehensive information for its serviceability quantification and maintenance scheduling [1]. Pavement condition evaluation is generally composed of two major procedures: the pavement distress evaluation, which is conducted to calculate the Distress Rate (DR), and the pavement roughness assessment, which is performed to retrieve the International Roughness Index (IRI). State transportation agencies are responsible for examining pavement conditions within their jurisdiction on a regular basis and performing the road-way maintenance and rehabilitation accordingly. Generally, pavement condition information is collected through manual evaluations or automatic techniques. In a manual evaluation procedure, an inspector walking along roads visually evaluates the severity and extent of pavement distresses based on pre-specified criteria [2]. However, manual evaluation is labor-intensive and time-consuming, and the inspector is often at high risk of being in an accident even with preventive safety measurements. With these disadvantages in mind, automatic pavement detection techniques have been developed and gained increasing popularity among state transportation agencies. Automated pavement condition data are generally collected with automated and dedicated devices, such as pavement scan vans or aerial photo cameras. However, regardless of the data collection procedures, the quality of the data collected is always compromised to some extent due to the individual subjectivity in evaluating the severity and extent of pavement distresses [3]–[5]. Therefore, computer-aided pavement distress detection and surface reconstruction methods are needed to minimize the impacts of human subjectivity in pavement condition distress assessments.

Considerable research has been conducted to assist pavement condition evaluation in using computer-aided techniques. For example, Tremblais and Augereau [6] proposed a fast multi-scale edge detection algorithm to detect pavement cracks. Bray *et al.* [7] proposed a neural network-based technique for an automatic classification of pavement cracks. Among all the existing computer-aided techniques, digital image processing is a mature method that has been increasingly utilized in pavement distress detection and road surface re-construction. Numerous studies have been conducted to improve the applicability and performance of image processing techniques for pavement surface evaluation. For instance, Mahler *et al.* [8] demonstrated the feasibility of using image processing techniques to detect cracks. Georgopoulos *et al.* [9] developed an image processing techniques to automatically determine the type, extent, and severity of surface cracks for flexible road pavements. Although a wide range of algorithms have been developed to improve the performance of image

Manuscript received April 30, 2015; revised December 9, 2015, March 21, 2016, September 10, 2016, January 26, 2017, and October 13, 2017; accepted December 28, 2017. Date of publication May 11, 2018; date of current version November 27, 2018. The Associate Editor for this paper was E. Kaisar. *(Corresponding authors: Guohui Zhang; Yin Yang.)*

Y. Zhang and Y. Yang are with the Department of Electrical and Computer Engineering, The University of New Mexico, Albuquerque, NM 87131 USA (e-mail: yangy@unm.edu).

Q. Lu is with the Department of Computer Science, The University of New Mexico, Albuquerque, NM 87131 USA.

S. Zhang is with the Department of Civil Engineering, University of New Mexico, NM 87131 USA.

C. Chen, Q. Wu, and G. Zhang are with the Department of Civil and Environmental Engineering, University of Hawaii at Manoa, Honolulu, HI 96822 USA (e-mail: guohui@hawaii.edu).

Color versions of one or more of the figures in this paper are available online at http://ieeexplore.ieee.org.

Digital Object Identifier 10.1109/TITS.2018.2791476

processing techniques in pavement distress evaluation, most of these are based on 2D image information. Distress depth is not able to be measured directly but only inferred from overlapping 2D images. Therefore, estimation errors would be inevitably introduced and evaluation accuracy would be degraded. Ideally, width and length, are two measurements to evaluate pavement distress severity and extent, and depth is generally used to determine pavement maintenance and rehabilitation [10]. Recent developments of 3D reconstruction approach enable a direct collection of 3D pavement distress information including not only width and but also the depth. 3D reconstruction relies on 3D point clouds (via inversely projecting the depth image pixels) collected by laser scanners or by stereo-vision algorithms-based video cameras [11]. In the past decades, significant effort has been taken to investigate the applicability of 3D reconstruction techniques in pavement condition evaluation [12]–[14]. For instance, Laurent *et al.* [12] used an auto-synchronized laser scanning system to detect road rutting and cracking in high precision 3D environments. Other studies were also proposed to improve the performance 3D reconstruction techniques [15]–[17]. These studies provided comprehensive and in-depth understandings of pavement condition evaluation and pavement surface in 2D and 3D reconstructions. However, these techniques are either not maturely developed or too costly in practical applications, which impede their wider implementations.

Microsoft Kinect is an infrared-based sensory device enabling human-computer interaction without the assistance of any physical controllers. It operates by capturing user gestures. Kinect is able to produce real-time 3D surface data and has been widely applied in many fields, such as physical re-habilitation, education, cartography, etc. Tölgyessy and Hubinskỳ [18] applied Kinect to robotics education, including data fusion, obstacle avoidance, collision detection, object recognition, gesture control, localization, and navigation. Compared to other aforementioned 3D reconstruction techniques, Kinect was originally developed for home entertainment and is very affordable at less than \$ 150 per unit. With its cost-effective and multi-disciplinary implementations, there is great potential to apply Kinect devices in pavement condition evaluations. This study is proposed to develop a cost-effective Kinect-based approach for 3D pavement surface reconstruction and cracking detection. Kinect fusion, point cloud conversion, mesh triangulation, and sharp feature examination modules are developed successively for crack recognition and severity identification. Human expert evaluation results are used as ground-truth data for comparison analyses. The results indicate that the proposed approach is able to re-construct 3D surfaces, detect crack width, length, and depth information, and further identify distress severity levels based on the given protocols.

The rest of the paper is organized as follows: a comprehensive literature review is provided in Section II. Section III introduces the Kinect fusion mechanism and the data collection procedure, followed by Section IV which details the methodology we adopted. Section V discusses the experiment results and research limitations, and this research is concluded with Section VI.

II. Previous Work

Pavement surface distress information is essential in the pavement management program. Various levels of pavement maintenance activities and rehabilitation decisions are supported by pavement condition information [19]. Federal and State Departments of Transportation (DOTs) in the U.S. have surveyed different types and numbers of distresses, and applied various pavement assessment approaches and pavement condition indices in their pavement evaluation procedures [4], [20]–[22]. For example at the federal level, the National Cooperative Highway Research Program (NCHRP) summarized existing data collection and processing techniques [22], as well as the data quality management issues and solutions [20] in automated pavement distress collection procedures. Meanwhile, at the state level, the Alabama Department of Transportation (ALDOT) utilizes manual evaluation methods in their pavement evaluation procedures. While manual surveys are still used among several states, the automated approaches have come into progressively more use. New Mexico Department of Transportation (NMDOT) applies both manual evaluation and automatic detection for pavement evaluation and uses a Pavement Serviceability Index (PSI) to measure pavement deterioration. Oregon Department of Transportation (ODOT) applies automated data collection equipment for pavement evaluation. Considerable studies have also been performed to explore advanced techniques for pavement distress detection and pavement condition evaluation. For example, acoustic or laser sensors have been used to capture pavement cracking, aiming to relate cracking to abrupt variations in pavement texture [21]. Analog approach refers to the process wherein images are physically imposed on film or another median, like photographic and video [23]–[26]. The data captured by digital imaging approach can be read electronically to be processed or reproduced. Pavement surface reconstruction is a major procedure in automatic pavement evaluation analysis. Zhang and Elaksher [27] developed image processing-based algorithms to quantify 3D details of pavement distresses using unmanned aerial vehicle (UAV) based image data. With a new image segmentation algorithm, Oh [28] developed an image processing method to automatically analyze the recorded images and isolate distress features. Pynn *et al.* [29] applied several new image processing algorithms to automatically detect the cracks by using video images collected with a van camera system. Pavement cracking, including longitudinal cracking, transverse cracking, alligator cracking and edge cracking, is a dominant category of pavement distress measurement, and the severity and extent of pavement cracking play significant roles in deteriorating pavement serviceability. Therefore, a significant amount of research has been conducted to improve pavement cracking detection and measurement from different perspectives. Zhou *et al.* [30] proposed a wavelet-based image classification algorithm to detect cracks in pavement surfaces. Huang and Xu [31] presented an image processing algorithm customized for high-speed, real-time inspection of pavement cracking. Mustaffara *et al.* [26] proposed a photogrammetry-based approach to automatically classify and quantify the pavement cracks. Ma *et al.* [32] proposed a method to detect cracks based on a non-subsampled contour transform algorithm. Oliveira and Correia [33] employed entropy and image dynamic thresholds to automatically segment road cracks. Chambon *et al.* [34] proposed to extract road cracks with adapted filtering and a Markov model-based segmentation. Distress depth information is an important contributing factor in determining pavement maintenance and rehabilitation [10]. However, traditional pavement evaluation and surface reconstruction methods are not able to capture depth information directly and accurately. In the last two decades, along with the advances of 3D surface reconstruction techniques, distress depth detection, especially crack depth detection, became feasible. 3D surface reconstruction relies on 3D point clouds collected by laser scanners or by stereo-vision algorithms using a multiple calibrated cameras [11]. Microsoft Kinect is an infrared-based motion sensor that is able to gather real-time 3D geometric feature, color, and audio data of the environment [35]. With the merits of its mature techniques and affordable expenses, Kinect has been applied in many fields. Chang *et al.* [36] examined the application of Kinect devices in physical rehabilitation and found that they can provide competitive motion tracking performance in the comparison to other professional motion detection systems. Lange *et al.* [37] investigated the interactive game-based re-habilitation using Kinect devices and proved their applicability in clinical use. Kitsunezaki *et al.* [38] performed a study of using Kinect for physical rehabilitation. Other research investigated the application of Kinect in education [39]. Ren *et al.* [40] investigated the application of Kinect hand gesture recognition function in human-computer interactions. Kondori *et al.* [41] studied the 3D head pose estimation using Kinect. Khoshelham and Elberink [42] studied the application of Kinect's depth data in the indoor mapping. Oliver *et al.* [43] investigated the application of Kinect as a navigation sensor for mobile robotics. Inspired by the great success of Kinect applications in these areas, this research proposed an innovative system for pavement surface reconstruction and cracking recognition.

A technical challenge of involving 3D sensors during pavement condition evaluation lies in the fact that these sensors inevitably induce more information to be processed. While there exist a wide range of algorithms for geometric analysis like manifold harmonics [44]–[46] or spherical harmonics [47], [48]. These methods are often *global* meaning they tend to obtain the most useful information based on the entire 3D model. This is clearly not the case of for the analysis of pavement distress. We show that by only examining local sharp features, we can robustly and accurately extract key parameters associated with pavement cracking.

III. Kinect-Based Data Collection

The Microsoft Kinect device (the first generation) is employed as the major sensor for data collection. Kinect was originally designed as a device for home entertainment since it enables human-computer interaction without additional controllers [35]. The Kinect sensor consists of an infrared (IR) laser emitter, an IR camera, and a regular RGB color camera. Besides the traditional RGB sensing with the resolution of 640×480 pixels at 30 frames per second. Kinect is also capable of sensing the depth information by tracking the emitted IR rays as shown in Fig 1. The geometry of the pavement surface can be further represented by converting the *level-set* surface representation [49] into a triangle mesh, consisting of small inter-connected triangle faces using the marching cube algorithm [50].

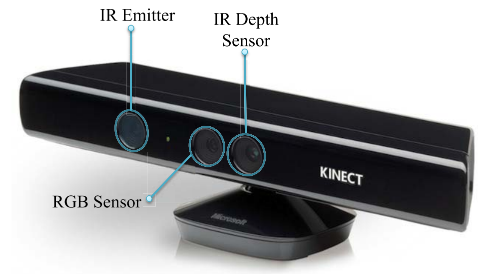

Fig. 1. The first generation of Microsoft Kinect sensor.

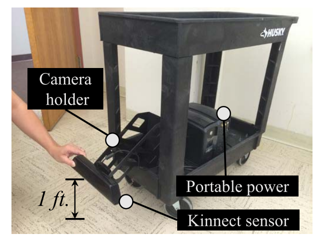

Fig. 2. Data collection setup.

In this study, the data of pavement cracks on road surfaces were collected at the University of New Mexico main campus and representative local streets and highways, including the segment of `Central Ave.` from `Washington St. NE` to `Broadway Blvd. SE` (a 23.1-mile long multi-lane highway, both Eastbound and Westbound directions), the segment of `Lomas Blvd. NE` from `San Mateo Blvd. NE` to `University Blvd. NE` (a 14.2-mile long multi-lane highway, both Eastbound and Westbound directions), the segment of `Girard Blvd. SE` from `Indian School Rd. NE` to `Gibson Blvd. SE` (a 22.5-mile long two-lane highways, both Northbound and Southbound directions) and the segment of `Yale Blvd. SE` from `Central Ave. SE` to `Gibson Blvd. SE` (a 3.5-mile long two-lane highway, both Northbound and Southbound directions) in the City of Albuquerque, NM.

To facilitate the procedure of data collection, a mobile data collection stand was built for mounting the Kinect during the pavement data collection on-site as shown in Fig. 2. There is a camera holder that fits the base of the attached Kinect sensor. The vertical distance between the camera to the floor is 1 ft., which allows us to use the *near mode* of the Kinect fusion [51] and improves the result. Two portable power supplies are also equipped on the stand. A `Lenovo Thinkpad T430` laptop computer equipped with an `Intel i7 CPU` and `16G RAM` was connected to the Kinect. Note that slight oscillations of the Kinect sensor during the data collection do not affect the accuracy or quality of the final reconstruction as the camera's position and orientation can be

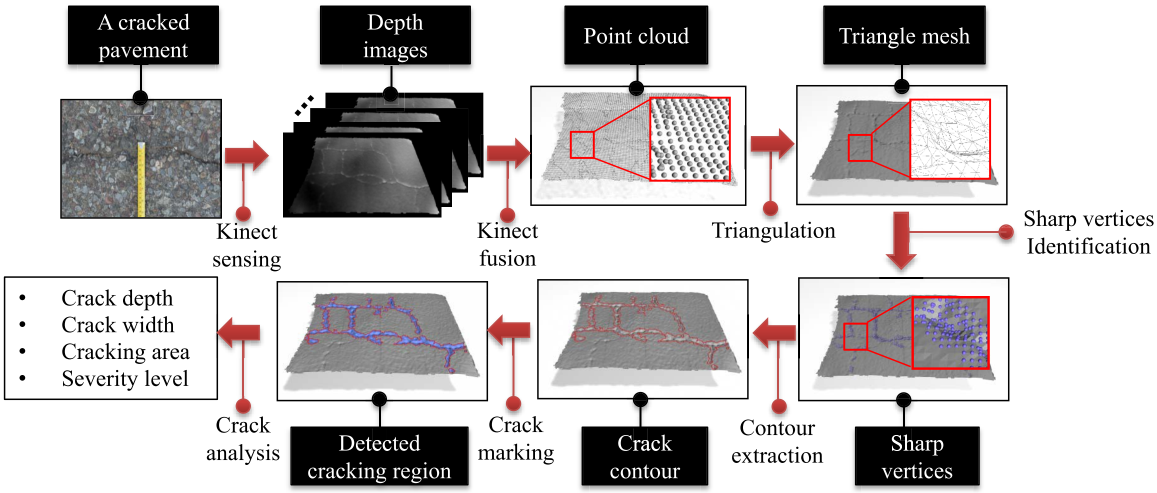

Fig. 3. An overview of the proposal framework of crack analysis.

dynamically tracked during the Kinect fusion [51]. Due to the hardware limitation, excessive darkness or brightness in the environmental ambient will degenerate the performance of the RGB camera. However, this issue can be easily fixed by adding artificial illumination when boarded on a moving van. Three types of pavement cracks were measured: 1) Longitudinal cracking refers to cracks that are predominantly parallel to the pavement centerline (or traffic direction) [2]; 2) Transverse cracking is the ones are predominantly perpendicular to the pavement centerline; 3) Alligator cracking corresponds to the cracks occur in areas subjected to repeated traffic loadings, especially along the wheel paths. In the early development stages, alligator cracking can appear as a series of interconnected seams. Eventually, they morph into many-sided, sharp-angled pieces, usually less than one foot on the longest side, characterized by a chicken wire/alligator skin pattern in the later stages. For each type of crack, 339 to 385 sample data were collected for cracking detection and analysis with a total of crack samples. The amount of cracking samples for each type on each severity was determined based on previous studies and statistical experiences [52], [53] Each record of a single pavement crack sample consists of a 3D mesh based on the captured Kinect depth streams. An evaluation from human experts was conducted as the ground truth through dedicated camera photographs taken for the same samples (Fig. 4). In order to distinguish longitudinal cracks from the transverse ones, the axis of a depth frame was aligned with the traffic direction. Thus, the direction of longitudinal cracks in the depth frame captured by Kinect is vertical and that of transverse cracks is horizontal. All the pavement data were collected on the dry surface of asphalt concrete pavement.

IV. Research Methodology

A. An Overview of System Framework

This paper aims to utilize the Microsoft Kinect (Fig. 1) to reconstruct pavement surfaces and capture geometric information of pavement cracking, including crack width, length, and depth. As sketched in Fig. 3, we developed a series of

Fig. 4. Expert evaluation is based on the pho-tograph from the dedicated professional camera of the crack site.

algorithms to facilitate an automatic identification of distress severities of three major types of pavement cracks to provide necessary information for pavement condition evaluation. Observing the fact that pavement cracks inevitably undermine the smoothness of the surface geometry, we devised a *local* algorithm that automatically screens all the potential *sharp vertices* on the mesh, where a salient surface geometry variation exists. This is accomplished by analyzing the distribution of normals of a small neighboring region surrounding a mesh vertex being examined. A breadth-first search (BFS) is used to obtain connected components out of all the sharp vertices. The cracking region can then be identified as the covered area of the largest connected vertices. The geometric parameters, such as the width, length, and depth of the cracks, are then calculated. Each step in Fig. 3 will be detailed in the following sub-sections.

B. Depth Retrieval and Surface Reconstruction

Although the Kinect sensor provides a fast dense depth sampling of its target's surface, the raw data could contain a significant amount of high-frequency noises and missing captures (e.g. holes on the surface). In addition, one Kinect frame is only able to sense the depth information of a small region, which is far from sufficient to completely cover an entire cracking site. To resolve this problem, we used a technique named Kinect fusion [52]. Kinect fusion "merges" the

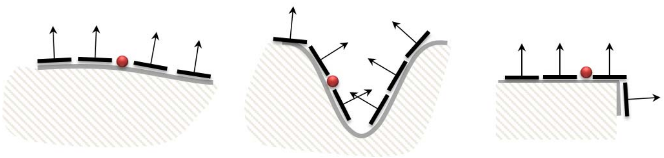

Fig. 5. Left: the normal directions of triangles close to a vertex (shown as a red sphere) on a smooth pavement surface are mostly in parallel. Middle: when it is close to a crack, normals are irregularly scattered. Right: a non-uniform normal distribution does not necessary mean sharp vertex.

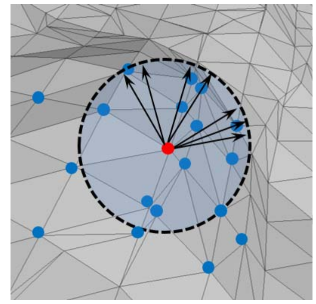

Fig. 6. DGM of a vertex (in red) on the mesh.

depth information from multiple Kinect frames. Specifically, for an incoming depth frame from Kinect sensor Kinect fusion first computes the corresponding camera pose, which can be encoded as a 4 by 4 homogeneous matrix. After un-projecting the depth points into 3D, a multi-resolution iterative closest point (ICP) method [54] is used to align the frame into a global 3D model (which is the pavement surface in our system) represented using the volumetric truncated signed distance function (TSDF) [55]. The constructed pavement mesh contains 3D geometry information of the pavement surface (we refer readers to related studies [52], [56] for a more detailed explanations of algorithmic procedures of Kinect fusion).

C. Feature Extraction

The concept of k-ring neighbor of a vertex on the mesh is frequently utilized in our feature extraction stage. Let $\mathcal{M}(\mathcal{E}, \mathcal{V})$ denote the triangle mesh, where $\mathcal{E}$ and $\mathcal{V}$ are sets of edges and vertices on $\mathcal{M}$. The *one-ring neighbor* $\mathcal{N}_1^{v_i}$ of a given vertex $v_i \in \mathcal{V}$ is a set of vertices such that $\forall v_j \in \mathcal{N}_1^{v_i}$, $\langle v_i, v_j \rangle \in \mathcal{E}$. The one-ring neighbor of all the vertices on the mesh can be easily found by iterating all the triangles on the mesh once, which is clearly an $\mathbf{O}(N)$ operation. Similarly, k-ring neighbor $\mathcal{N}_k^v$ of vertex v is defined as a set of vertices such that they can be reached from by traveling through v at most k edges on the mesh. The k-ring face $\mathcal{F}_k^v$ is the set of triangles such that each of its triangles holds at least one element in $\mathcal{N}_k^v$. As such neighboring information of vertices will be used repeatedly, we assign each vertex a linked list storing $\mathcal{N}_k^v$ and $\mathcal{F}_k^v$ immediately after the triangle mesh is reconstructed.

The next step is to identify the locations corresponding to the cracks on the constructed 3D surface. It is assumed that an intact pavement surface is smooth indicating that the normal of nearby triangles should be in the similar direction. On the other hand, the location close to the crack is more likely to have irregular distribution of normals as shown in Fig. 5 left and middle. To evaluate the smoothness of a neighbor region of a vertex, the flatness test is performed by computing an area-weighted averaged normal direction for all the triangles that are close to a certain mesh vertex (e.g. defined using ring neighbor of such that:

$$\bar{\mathbf{n}} = \frac{\sum_{F_i \in \mathcal{F}_k^v} A(F_i) \cdot \mathbf{n}(F_i)}{\sum_{F_i \in \mathcal{F}_k^v} A(F_i)} \tag{1}$$

Here, $\mathbf{n}(F_i) \in \mathbb{R}^3$ is the unit 3 by 1 normal vector of F_i, a triangle of the k-ring neighbor of vertex v. $A(F_i)$ represents the area of F_i. It is noteworthy that $\bar{\mathbf{n}}$ does not have to be a unit vector. Afterwards, we computed the "distance" between $\mathbf{n}$ and $\bar{\mathbf{n}}$ using the angle α_i between them:

$$\alpha_i = \arccos\left(\frac{\bar{\mathbf{n}} \cdot \mathbf{n}(F_i)}{|\bar{\mathbf{n}}|}\right) \tag{2}$$

Finally, the standard deviations (SD) among all the calculated α_i are evaluated. If the SD is lower than a given threshold, all the triangles in $\mathcal{F}_k^v$ are regarded as *flat* and being free of cracks. Otherwise, F_i could potentially be associated with sharp features (e.g. edges of the crack) and further analysis would be necessary. We found that the flatness test based on two or three-ring neighbors can effectively remove most smooth vertices.

The discrete Gauss map (DGM) [57] is employed for further investigations of the local geometry feature associated with v that fails the flatness test. In DGM, a unit sphere centered at v is defined and each $F_i \in \mathcal{F}_k^v$ is mapped to a point p_i on the sphere's surface by travelling from v along $\mathbf{n}(F_i)$ for a unit distance. This can be computed via:

$$\mathbf{p}_i \triangleq DGM(F_i, v) = \mathbf{v} + \mathbf{n}(F_i), \quad F_i \in \mathcal{F}, \tag{3}$$

where $\mathbf{p}_i, \mathbf{v} \in \mathbb{R}^3$ are the 3D positions of p_i and v. Fig. 6 shows an illustrative example of the DGM for a vertex (the red vertex) on the mesh. We reorganize the mapped points on the sphere into clusters such that points within a cluster are closer to each other. It is clear that if v happens to sit on the intersection of two planes, its neighboring faces should hold two distinctive normal directions. Accordingly, its DGM points can be grouped into two clusters. Similarly, three DGM clusters indicate an intersection by three planes of different orientations. However, if the number of resulting clusters is larger than four, it is more likely that is on a rough surface rather than a sharp feature as we rarely have intersections of more than four planes on the roadway pavement. The major calculation in the DGM clustering is to measure the "distance" between two DGM points. As each point actually represents a normal vector of a triangle in $\mathcal{F}_k^v$, the regular Euclidean distance is obviously not a good choice. Alternatively, we use the *geodesic distance* on the sphere (e.g. the great-arc length), which equals the minimal angle between the two normal vectors and can be computed as:

$$dist_g\left(p_i, p_j\right) = \arccos\left(\mathbf{n}(F_i) \cdot \mathbf{n}(F_j)\right). \tag{4}$$

At the beginning, each DGM point is assigned to a different cluster. The distance between two clusters $\mathcal{C}_i$ and $\mathcal{C}_j$ is defined as the maximum distance between all the DGM point pairs from each cluster:

$$dist\left(\mathcal{C}_i, \mathcal{C}_j\right) = \max_{p_n \in \mathcal{C}_i, p_m \in \mathcal{C}_j} dist_g\left(p_n, p_m\right), \tag{5}$$

where p_n and p_m are DGM points from $\mathcal{C}_i$ and $\mathcal{C}_j$ respectively. As long as $dist(\mathcal{C}_i, \mathcal{C}_j)$ is smaller than a sensitivity parameter α_t, they will be merged into a new cluster. We keep merging all clusters until the distance between any pair of the clusters is larger than α_t. If the final number of the cluster is between two and four, υ is considered a *sharp vertex*.

D. Crack Analysis

Although our method is able to mark most vertices on cracks as sharp vertices, some vertices away from cracks may also be mistakenly labeled due to the regional pavement roughness. Therefore, we need to further extract vertices that truly belong to the crack. This was achieved by applying a BFS over all the sharp vertices detected in the previous step based on the assumption that the crack region should be the most dominant geometry feature on the pavement segment of interest. BFS algorithm retrieves all the connected components on the mesh, where a connected component is a subset of vertices and edges such that any two vertices can be reached through its edge set. The connected components of small size (e.g. smaller than 1,000 sharp vertices) are most likely associated with some minor surface dents rather than cracks. Therefore, they are discarded (as shown in Fig. 7 (a)). The triangle incident to a sharp vertex is labeled as *sharp face*. Due to the strong connectivity of the connected component, it is guaranteed that all the triangles associated to a connected component are also connected and formed a sub-mesh or the cracking region. The contour of the crack region can be easily extracted by iterating all the edges: a contour edge is the one shared by two triangles such that one of the triangles is a sharp feature face while the other one is not. In order to make the framework directly useful for the pavement evaluation, detailed parameters and statistics, such as the width, length, and depth of cracks, must be automatically reported out of the crack region marked. This feature is also supported in our framework.

1) Crack Depth: It seems that the crack depth could be directly obtained by looking at the values of the sharp vertices within a crack region. Unfortunately, it is not always the case that the pavement surface perfectly aligns with the plane of the camera coordinate frame (CCF). In most situations, the pavement of the road formed an arch and the depth of the crack was actually the distance from the valley of the crack to the tangent plane of the surface. Based on this observation, we used the least square fitting (LSF) sphere surface to approximate the pavement arch. The LSF sphere is described by the standard sphere equation as:

$$x^2 + y^2 + z^2 - Ax - By - Cz + D = 0, \tag{6}$$

where A, B, C, D are four unknown coefficients to be determined. The quadratic equation is optimal (best fitting)

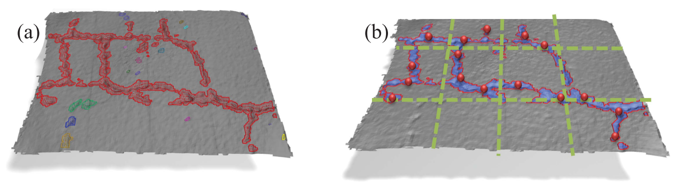

Fig. 7. (a) The result of BFS on a pavement mesh. The red regions are the large connected component. Other small components in other colors are discarded. (b) Crack depth evaluation by grids. At each grid, the deepest sharp vertices are picked (red spheres) for local depth evaluation.

when the sum of the squared distance from vertices to sphere surface is minimized:

$$\arg\min_{A,B,C,D} E, \quad E = \sum \left(x_i^2 + y_i^2 + z_i^2 - Ax_i - By_i - Cz_i + D\right)^2, \tag{7}$$

where x_i, y_i and z_i are the x, y and z coordinates of a vertex υ. Because sharp vertices are located at the valley/edge of the crack far away from the pavement surface, they should not participate in LSF sphere equation evaluation. Accordingly, the summation in Eq. (7) only takes over all the non-sharp vertices. Unknown parameters A, B, C and D can be solved by setting the gradient of E as $\mathbf{0}$:

$$\Delta E = \left[\frac{\partial E}{\partial A}, \frac{\partial E}{\partial B}, \frac{\partial E}{\partial C}, \frac{\partial E}{\partial D}\right] = \mathbf{0}, \tag{8}$$

which yields a 4×4 linear system:

$$\begin{bmatrix} \sum x_i^2 & \sum x_i y_i & \sum x_i z_i & -\sum x_i \\ \sum x_i y_i & \sum y_i^2 & \sum y_i z_i & -\sum y_i \\ \sum x_i z_i & \sum y_i z_i & \sum z_i^2 & -\sum z_i \\ -\sum x_i & -\sum y_i & -\sum z_i & \sum 1 \end{bmatrix} \begin{bmatrix} A \\ B \\ C \\ D \end{bmatrix} = \begin{bmatrix} \sum x_i(x_i^2 + y_i^2 + z_i^2) \\ \sum y_i(x_i^2 + y_i^2 + z_i^2) \\ \sum z_i(x_i^2 + y_i^2 + z_i^2) \\ -\sum x_i(x_i^2 + y_i^2 + z_i^2) \end{bmatrix} \tag{9}$$

Lastly, the depth of a vertex υ on the mesh is defined as the distance to the LSF sphere surface:

$$depth(\upsilon) = R - \sqrt{(x - x_o)^2 + (y - y_o)^2 + (z - z_o)^2}, \tag{10}$$

where x_o, y_o and z_o are the coordinates of the center of the sphere. R is the radius of the sphere. The crack depths at different regions could be different. We regularly partitioned the pavement mesh into by grids. The top 5% of the deepest sharp vertices computed via Eq. (10) serve as representative depth samples at each local grid cell. The average of them is then used for the final crack depth estimation as shown in Fig. 7 (b).

2) Crack Width: Evaluating the average crack width is challenging especially for cracks with irregular patterns. As shown in Fig. 8, the red dot is a local deepest sharp vertex within a grid cell, which is assumed to be located at the valley of the crack. Its nearby surface vertices are shown as blue dots. The projection of the vector pointing from the sharp vertex to its

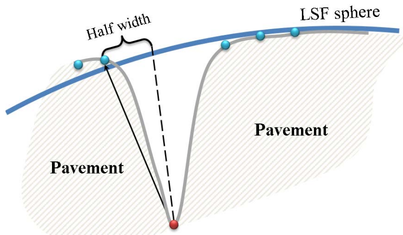

Fig. 8. Width measurements.

closest surface vertex on the LSF sphere surface provides us a reasonable approximation of the half width of the crack. As a result, the local crack width at the grid was computed as:

$$width(v) = 2|\mathbf{v}' - \mathbf{v}'_S|, \tag{11}$$

where $\mathbf{v}', \mathbf{v}'_S \in \mathbb{R}^3$ are 3D positions of the deepest sharp vertex and its closest projected crack boundary vertex. In our implementation, we use the three nearest crack boundary vertices for a better width approximation.

3) Crack Length & Area: The area of the crack is just the summation of the area of all the sharp faces projected to the LSF sphere. The length can be computed by dividing the crack area by its average width. Finally, the severity of the crack can be estimated based on the evaluated crack parameters.

V. Experimental Tests and Discussions

A. Surface Reconstruction

With the help of Kinect fusion technique, the 3D reconstruction can be made for a wide pavement surface area. Indeed, we can reconstruct arbitrarily wide and lengthy pavement as long as there is sufficient hard drive space. After the mesh reconstruction is completed, the aforementioned feature detection and crack analysis algorithm will be applied. It is also easy to see that, all the calculation for extracting crack's geometry is essentially local, meaning the entire analysis is an $\mathbf{O}(N)$ linear algorithm. The calculated crack parameters (width, length and depth) are used following the existing flexible pavement evaluation standard in New Mexico [2] to assess the severity of each crack sample. Such results are further compared with manual severity estimation by experts for algorithm performance assessment.

We also created an online database using a `WebGL` based interface (http://ece-research.unm.edu/yyang/pavement/), which can be assessed by the readers for free to further test our algorithms. The red spots on the map interface (supported by `Google Map API`) on the left corresponds to a crack site and its street view is provided at the bottom left corner. In the middle, the list of data from this site is provided and users can click on any of them to download it. Each item consists of a 3D mesh as shown in the rendering panel on the right and a photo with sample ID.

B. Accuracy Experiment

The suggested range of the first generation Kinect sensor is between 0.3 to 3 meters (i.e. 11.9–118 inches) when the *near*

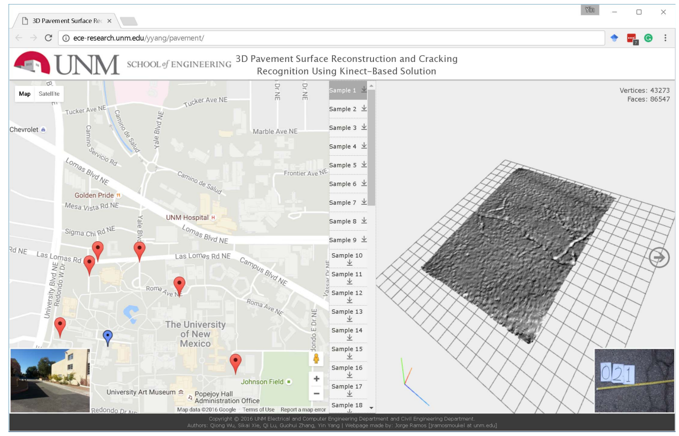

Fig. 9. A `WebGL` based database for collected cracking samples, available at http://ece-research.unm.edu/yyang/pavement/.

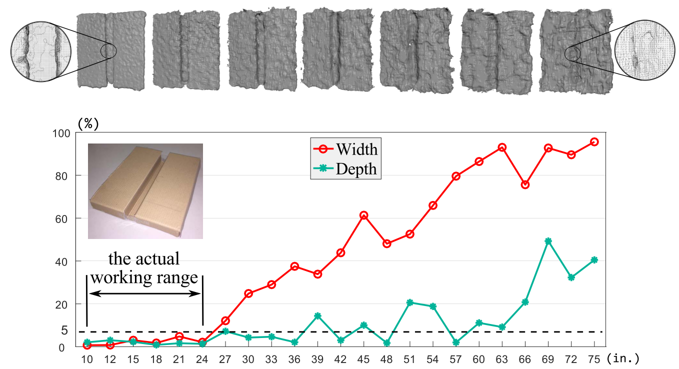

Fig. 10. In the phantom study, we test the accuracy of the proposed algorithm using a standard man-made cracking surface. While the relative error goes up when the Kinect moves further and further away from the phantom surface, the accuracy of our algorithm is typically below 5% if the Kinect-phantom distance is between 10 to 30 inches, within which is how our data collection was set. The reconstructed surfaces are also given in top.

mode is on. The phantom study tests the accuracy of the Kinect senor with a simple man-made cracking surface. As shown in the Fig. 10, the phantom was made of a cardboard with a one-inch wide and one-inch deep artificial dent at its middle. We compare the width/depth information calculated with the proposed algorithm on the digital reconstruction from the Kinect. Since the ground truth value is precisely known, this simple phantom study allows a quantitative understanding of the accuracy of the proposed algorithm. The result is reported in Fig. 10, where we plot the relation between the Kinect-phantom distance and the relative error between the calculated depth/width and the ground truth. It can be seen from the figure that the relative error of our algorithm based on the Kinect fusion is always less than 5% if the Kinect-phantom distance is between 10 inches to 30 inches, which is the typical working distance in our data collection (e.g. see Fig. 2). It is not surprising that if this distance increases, the quality of the resulting reconstruction is downgraded (as shown in Fig. 10 top). Thus the relative error goes up accordingly.

To further illustrate the versatility of our algorithm, we also did a side-by-side comparison applying the proposed method

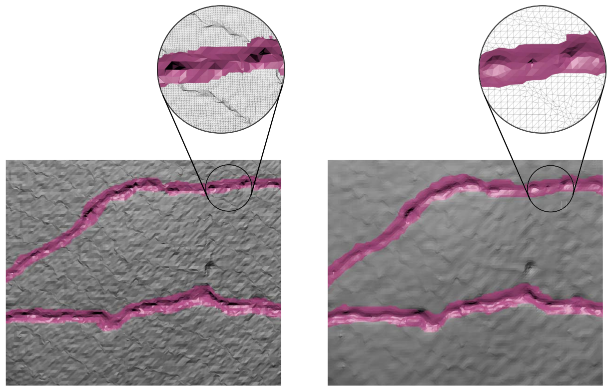

Fig. 11. Side-by-side results of the crack detection with the proposed algorithm using LIDAR (left) and Kinect (right) data.

to 3D surface geometries obtained from both LIDAR and Kinect. For the LIDAR, a Delaunay triangulation [58] was performed the construct the corresponding mesh. It can be clearly seen from the Fig. 11 that while the quality of Kinect data is not as superior as the ones from the professor LIDAR sensor. The cracking region is still correctly detected regardless the resolutions of the input meshes. The experiment validates the robustness of our algorithm.

C. Test Results for Various Cracking Detection

The proposed system is able to capture the shape information of various cracks. Before being analyzed by the proposed Kinect fusion and crack detection technique, all the collected crack sample data were manually examined by trained pavement inspectors, and their severity evaluation results, after agreeable adjustments, were used as observed truth data for performance assessment purposes. The data collection was carried by three sensor Ph.D. students and two professors. All the members went through a two-day training workshop provided by NMDOT. The geometry measure of the cracks were all obtained in the field. Table I reports the performance of the proposed approach and the confusion matrix for transverse cracking regarding each severity as well as failure detection. Tables II and III demonstrate these summaries for longitudinal cracking and alligator cracking. In these tables, each row represents the number of observed instances for each severity level, and each column illustrates the number of predicted instance for each severity and failure detection. The last two columns list the *true positive rate* (TPR) and *failure detection rate* (FDR) for each crack severity. TPR measures the proportion of actual positives which are correctly identified as such (i.e. the proportion of Severity 1 samples that are correctly identified as Severity 1), and FDR denotes the proportion of records that failed to identify. The three tables show that the proposed method was able to correctly identify 78.27% of longitudinal cracking, which is the highest of all the three major cracking types, and it per-forms relatively inferiorly on alligator cracking detection, with the lowest TPR of 55.16%. In the meantime, the proposed method failed to identify a small amount of collected samples for each cracking type, indicated by the overall FDR. With comparable sample size for each cracking type, the proposed approach

TABLE I

TRANSVERSE CRACKING SEVERITY DETECTION RESULTS

Observed Samples by Severity	**Predicted Samples by Severity**				**TPR**	**FDR**
	Severity 1 (104)	Severity 2 (149)	Severity 3 (90)	**FD** (42)		
Severity 1 (160)	101	45	1	13	63.13%	8.13%
Severity 2 (113)	3	81	11	18	71.68%	15.93%
Severity 3 (112)	0	23	78	11	69.64%	9.82%
Total 385	260 (Total correct predictions)			42	67.53%	10.91%

TABLE II

LONGITUDINAL CRACKING SEVERITY DETECTION RESULTS

Observed Samples by Severity	**Predicted Samples by Severity**				**TPR**	**FDR**
	Severity 1 (110)	Severity 2 (146)	Severity 3 (79)	**FD** (42)		
Severity 1 (144)	109	31	1	3	75.69%	2.08%
Severity 2 (113)	1	99	5	8	87.61%	7.08%
Severity 3 (102)	0	16	73	13	71.57%	12.75%
Total 359	281 (Total correct predictions)			24	78.27%	6.69%

TABLE III

ALLIGATOR CRACKING SEVERITY DETECTION RESULTS

Observed Samples by Severity	**Predicted Samples by Severity**				**TPR**	**FDR**
	Severity 1 (69)	Severity 2 (142)	Severity 3 (98)	**FD** (30)		
Severity 1 (119)	65	31	5	18	54.62%	15.13%
Severity 2 (128)	4	73	44	7	57.03%	5.47%
Severity 3 (92)	0	38	49	5	53.26%	5.43%
Total 339	187 (Total correct predictions)			30	55.16%	8.85%

has the highest amount (42 samples) and FDR (10.91%) for transverse cracking, and close recognition performance on longitudinal cracking (24 samples, 6.69%) and alligator cracking (30 samples, 8.85%). These results suggest that TPR and FDR are effective indices measuring the performance from certain aspects and should both be utilized for pavement cracking detection and evaluation.

The performance of the proposed method also varies for the same type of cracking with different severities. Taking Table I as an example, it shows that for transverse cracking, the proposed approach performs best on Severity 2 and is able to correctly classify 71.68% of all Severity 2 samples, followed by a comparable performance on Severity 3 (69.64%). It performs worst on Severity 1, with a TPR of 63.13%. This implies that the proposed approach is relatively better able to classify transverse cracks of higher severities. However, similar to the overall performance, it was also found that the pro-posed method is unable to recognize some of the cracks regarding each severity. Overall, the proposed approach is able to identify 89.09% (FDR = 10.91%) of all the transverse crack samples and is capable of correctly classifying 67.53% of all the transverse cracks, indicating an acceptable prediction performance. As is shown in Table I, this method fails to identify 8.13% of the Severity 1 transverse cracking, which is the least of all the three severities, followed by failure detections on Severity 3 (9.82%) and Severity 2 (15.93%). It is suggested that the proposed approach performs worst on recognizing Severity 2 transverse cracking, but in the meantime works

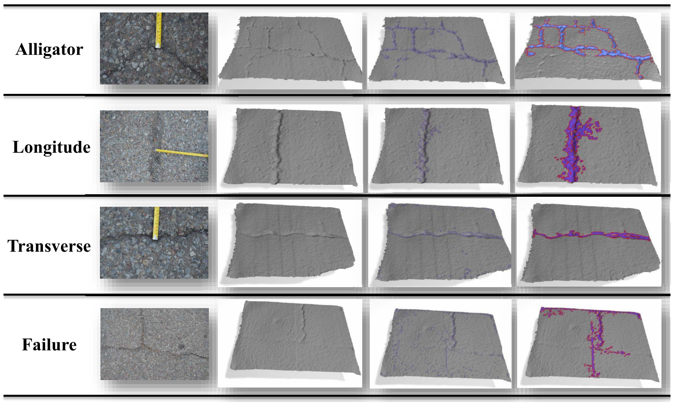

Fig. 12. More results from our method.

best after Severity 2 cracking is recognized, as is shown by the TRP. The crack detection results for longitudinal cracking and alligator cracking could be interpreted analogously, and therefore are omitted in this discussion.

It is also displayed in Table I that the proposed method tends to overestimate transverse cracks in Severity 2 and underestimate those in Severities 1 and 3. Specifically, there are a considerable amount of misclassified instances in each pair of severities: 45 samples of Severity 1 are misclassified as Severity 2 and 1 sample of Severity 1 is misclassified as Severity 3; 3 Severity 2 records are misclassified as Severity 1 and 11 Severity 2 samples are misclassified as Severity 3; 23 Severity 3 records are misclassified as Severity 2. It is also revealed that there is overall only 1 misclassification between Severity 1 and Severity 3, indicating a significant discrepancy between these two severity levels and that the proposed method is effective in detecting this discrepancy. The misclassifications for longitudinal cracking and alligator cracking, which are illustrated in Table II and Table III respectively, could be analyzed accordingly.

According to existing flexible pavement evaluation protocol in New Mexico [2], crack width is the major parameter used to define crack severity. Therefore, in this study, the crack width information is used in the severity classification process. However, it should be noted that both crack length and width are important parameters for pavement distress evaluation and therefore are also calculated by the proposed algorithm. Based on existing flexible pavement evaluation protocol, crack length is an important measurement to define pavement cracking extent. The cracking extent is not evaluated in this research, but the length information for each crack sample is extracted to verify the applicability of the proposed approach. Besides, the most critical problem affecting the pavement service life is the formation and growth of tracks due to physical stress and chemical deterioration. Therefore, crack depth is generally used a factor to determine pavement surface maintenance and rehabilitation [10]. Taking this into account, this study also extracts crack depth information, which may provide instructive reference for pavement surface maintenance schedule optimization.

Fig. 12 shows the result of three successful detections of alligator cracking, longitudinal cracking, and transverse cracking, respectively. We can see that the crack region is accurately identified and cracking features are explicitly characterized. It is demonstrated that the Kinect fusion algorithm and crack detection techniques are able to capture the shape information of various cracks. However, our method could also underperform in some extreme cases, where the crack is shallow and some regular surface roughness could present as significant geometry variations as the crack does. Therefore, high-level noise (fake sharp vertices) could be observed in the failure example as the bottom row in Fig. 12. The crack has less depth and width magnitude compared to the successful example, indicating that crack depth and width are significant factors related to successful crack detection. It also indicates that our system performs better on higher severities than lower severities, which is reasonable as the high severity crack is usually associated with width, length or depth of larger magnitude. Overall, the developed Kinect fusion technique and crack detection algorithms are able to detect three major types of pavement cracks. The proposed approach provides a viable alternative for pavement crack detection.

D. Limitations

While our experiment reports promising results, there still exist some limitations in the current version of our system, which leave us many exciting further directions to explore. First of all, we were using the first generation of Microsoft Kinect in this work. By the time of this paper submission, the second generation of Kinect had just been released, with higher depth resolution and frame rates. We will adapt our system to the latest Kinect hardware in the near future and a much more detailed surface reconstruction is expected. Second, our feature detection method works well for local sharp geometry features. However, lower performance was observed for subtle surface roughness and global shape variation (e.g. on a wide and smoothly curved surface). It is necessary to investigate new geometric analysis method to detect the cracks on the reconstructed pavement surface. Using spectral geometry analysis [17] is a promising further direction. Currently, we perform the crack analysis purely based on the reconstructed 3D mesh surface. We believe that by combining information from other data resources e.g. the classic RGB video camera [7], the accuracy of the pavement analysis can be further improved. We will also explore further possible enhancement of our current algorithm for instant, to use extended ICP algorithm [16] to improve the precision of the 3D construction from depth frames. Of course, the algorithm becomes more expensive and we may need to utilize find a better parallelization on general-purpose graphics processing unit (GPGPU) to further acceleration the processing speed [15]. Moreover, there is still limitation regarding Kinect field of view in this study, due to which examination of crack extent is not applicable. A possible solution, as was proposed in a previous study, is to use an array of Kinect to cover larger areas in both longitudinal and transverse directions. We also plan to install the Kinect to the vehicle to collect more 3D geometry data of the local streets and highways. In order to do that, we need to study how to de-blur the depth data when the Kinect sensor undergoes a fast movement. This may be achieved by fusing information from multiple Kinect devices.

VI. Conclusion

This study applies Microsoft Kinect, a consumer-level motion sensing input device to detect the geometric features, including width, length, and depth of different types of pavement distress. Research results indicate that Microsoft Kinect produces reliable geometric information of pavement distress and is able to report distress severity with a promising accuracy. Crack depth and width are significant factors related to successful crack detection indicated by the comparison of successful detection and failure detection examples, which demonstrates that Kinect crack detection algorithms perform better on higher severities than lower severities. Research limitations regarding the hardware constraint, method universal application, and data accessibility are also discussed. The main advantage of the proposed method includes two aspects: first, comparing with existing automatic pavement evaluation method, the proposed approach captures 3D pavement crack image and extract crack depth information, which is an important measurement to define pavement cracking severity. Besides, comparing with recently proposed advanced 3D surface reconstruction techniques, the Kinect fusion technique is consumer-level efficient and practice-ready, and has shown great potential for mass implementation with further improvement. Due to the hardware constraints and complicated data processing it is unlikely that the Kinect could completely replace the current state-of-the-art systems for pavement condition evaluation. Nevertheless, we believe the proposes system still provides an applicable complementary solution for automatic pavement evaluation, pavement surface 3D reconstruction, and distress severity quantification.

References

[1] C. Chen, S. Zhang, G. Zhang, S. M. Bogus, and V. Valentin, "Discovering temporal and spatial patterns and characteristics of pavement distress condition data on major corridors in New Mexico," *J. Transp. Geograph.*, vol. 38, pp. 148–158, Jun. 2014.

[2] P. Bandini, S. B. Halter, K. R. Montoya, Hung V. Pham, and G. Migliaccio, "Improving NMDOT's pavement distress survey methodology and developing correlations between FHWA's HPMS distress data and PMS data," Tech. Rep., 2012.

[3] J. Daleiden, "Variability of pavement distress data from manual surveys," in *Proc. Pavement Eval. Conf.*, 2014.

[4] S. Bogus, G. Migliaccio, and A. Cordova, "Assessment of data quality for evaluations of manual pavement distress," *Transp. Res. Rec., J. Transp. Res. Board*, vol. 2170, pp. 1–8, Nov. 2010.

[5] B. S. Underwood, Y. R. Kim, and J. Corley-Lay, "Assessment of use of automated distress survey methods for network-level pavement management," *J. Perform. Construct. Facilities*, vol. 25, no. 3, pp. 250–258, 2010.

[6] B. Tremblais and B. Augereau, "A fast multi-scale edge detection algorithm," *Pattern Recognit. Lett.*, vol. 25, no. 6, pp. 603–618, 2004.

[7] J. Bray, B. Verma, X. Li, and W. He, "A neural network based technique for automatic classification of road cracks," in *Proc. IEEE Int. Joint Conf. Neural Netw.*, Jul. 2006, pp. 907–912.

[8] D. S. Mahler, Z. B. Kharoufa, E. K. Wong, and L. G. Shaw, "Pavement distress analysis using image processing techniques," *Comput.-Aided Civil Infrastruct. Eng.*, vol. 6, no. 1, pp. 1–14, 1991.

[9] A. Georgopoulos, A. Loizos, and A. Flouda, "Digital image processing as a tool for pavement distress evaluation," *J. Photogramm. Remote Sens.*, vol. 50, no. 1, pp. 23–33, 1995.

[10] J. J. Lu, X. Mei, and M. Gunaratne, "Development of an automatic detection system for measuring pavement crack depth on Florida roadways," Tech. Rep., 2002.

[11] C. Koch and I. Brilakis, "Pothole detection in asphalt pavement images," *Adv. Eng. Inf.*, vol. 25, no. 3, pp. 507–515, 2011.

[12] J. Laurent, M. Talbot, and M. Doucet, "Road surface inspection using laser scanners adapted for the high precision 3D measurements of large flat surfaces," in *Proc. Int. Conf. Recent Adv. 3-D Digit. Imag. Modeling*, 1997, pp. 303–310.

[13] L. Bursanescu, M. Bursanescu, M. Hamdi, A. Lardigue, and D. Paiement, "Three-dimensional infrared laser vision system for road surface features analysis," in *Proc. 6th Conf. Opt. (ROMOPTO)*, 2001, pp. 801–809.

[14] S.-J. Yu, S. R. Sukumar, A. F. Koschan, D. L. Page, and M. A. Abidi, "3D reconstruction of road surfaces using an integrated multi-sensory approach," *Opt. Lasers Eng.*, vol. 45, no. 7, pp. 808–818, 2007.

[15] C. Langis, M. Greenspan, and G. Godin, "The parallel iterative closest point algorithm," in *Proc. 3rd Int. Conf. 3-D Digit. Imag. Modeling*, 2001, pp. 195–202.

[16] D. Haehnel, S. Thrun, and W. Burgard, "An extension of the ICP algorithm for modeling nonrigid objects with mobile robots," in *Proc. IJCAI*, vol. 3. 2003, pp. 915–920.

[17] J. Hu and J. Hua, "Salient spectral geometric features for shape matching and retrieval," *Vis. Comput.*, vol. 25, nos. 5–7, pp. 667–675, 2009.

[18] M. Tölgyessy and P. Hubinskỳ, "The Kinect sensor in robotics education," in *Proc. 2nd Int. Conf. Robot. Edu.*, 2011, pp. 143–146.

[19] R. Haas, W. R. Hudson, and J. P. Zaniewski, *Modern Pavement Management*. 1994.

[20] G. W. Flintsch and K. K. McGhee, "Quality management of pavement condition data collection," in *Transportation Research Board*, vol. 401. 2009.

[21] W. Gramling, "NCHRP synthesis of highway practice 203: Current practices in determining pavement condition," TRB, Nat. Res. Council, Washington, DC, USA, Tech. Rep., 1994.

[22] K. H. McGhee, "Automated pavement distress collection techniques," in *Transportation Research Board*, vol. 334. 2004.

[23] R. E. Smith, T. J. Freeman, and O. J. Pendleton, "Evaluation of automated pavement distress data collection procedures for local agency pavement management," Dept. Washington State Transp., Olympia, WA, USA, Tech. Rep. GC10470, 1996.

[24] K. C. Wang and O. Smadi, "Automated imaging technologies for pavement distress surveys," Transp. Res. E-Circular, Washington, DC, USA, Tech. Rep. (E-C156), 2011.

[25] W. L. Gramling and J. E. Hunt, "Photographic pavement distress record collection and transverse profile analysis," Strategic Highway Res. Program, Nat. Res. Council, Washington, DC, USA, Tech. Rep., 1993.

[26] M. Mustaffara, T. Lingb, and O. Puanb, "Automated pavement imaging program (APIP) for pavement cracks classification and quantification-a photogrammetric approach," *Int. Arch. Photogram., Remote Sens. Spatial Inf. Sci.*, vol. 37, no. B4, pp. 367–372, 2008.

[27] C. Zhang and A. Elaksher, "An unmanned aerial vehicle-based imaging system for 3D measurement of unpaved road surface distresses1," *Comput.-Aided Civil Infrastruct. Eng.*, vol. 27, no. 2, pp. 118–129, 2012.

[28] H. Oh, "Image processing technique in automated pavement evaluation system," Ph.D. dissertation, Univ. Connecticut, Storrs, CT, USA, 1998.

[29] J. Pynn, A. Wright, and R. Lodge, "Automatic identification of cracks in road surfaces," in *Proc. 7th Int. Conf. Image Process. Appl.*, vol. 2. 1999, pp. 671–675.

[30] J. Zhou, P. Huang, and F.-P. Chiang, "Wavelet-based pavement distress classification," *Transp. Res. Rec., J. Transp. Res. Board*, vol. 1940, pp. 89–98, Jan. 2005.

[31] Y. Huang and B. Xu, "Automatic inspection of pavement cracking distress," *J. Electron. Imag.*, vol. 15, no. 1, p. 013017, 2006.

[32] C.-X. Ma, C.-X. Zhao, and Y.-K. Hou, "Pavement distress detection based on nonsubsampled contourlet transform," in *Proc. Int. Conf. Comput. Sci. Softw. Eng.*, vol. 1. 2008, pp. 28–31.

[33] H. Oliveira and P. L. Correia, "Identifying and retrieving distress images from road pavement surveys," in *Proc. 15th IEEE Int. Conf. Image Process.*, Oct. 2008, pp. 57–60.

[34] S. Chambon, C. Gourraud, J. M. Moliard, and P. Nicolle, "Road crack extraction with adapted filtering and Markov model-based segmentation: Introduction and validation," in *Proc. Int. Joint Conf. Comput. Vis. Theory Appl. (VISAPP)*, 2010.

[35] A. Sanna, F. Lamberti, G. Paravati, and F. D. Rocha, "A Kinect-based interface to animate virtual characters," *J. Multimodal User Interfaces*, vol. 7, no. 4, pp. 269–279, 2013.

[36] C.-Y. Chang *et al.*, "Towards pervasive physical rehabilitation using Microsoft Kinect," in *Proc. 6th Int. Conf. Pervasive Comput. Technol. Healthcare (PervasiveHealth) Workshops*, 2012, pp. 159–162.

[37] B. Lange *et al.*, "Interactive game-based rehabilitation using the Microsoft Kinect," in *Proc. IEEE Virtual Reality Workshops (VRW)*, Mar. 2012, pp. 171–172.

[38] N. Kitsunezaki, E. Adachi, T. Masuda, and J.-I. Mizusawa, "Kinect applications for the physical rehabilitation," in *Proc. IEEE Int. Symp. Med. Meas. Appl. (MeMeA)*, May 2013, pp. 294–299.

[39] H.-M. J. Hsu, "The potential of Kinect in education," *Int. J. Inf. Edu. Technol.*, vol. 1, no. 5, p. 365, 2011.

[40] Z. Ren, J. Meng, and J. Yuan, "Depth camera based hand gesture recognition and its applications in human-computer-interaction," in *Proc. 8th Int. Conf. Inf., Commun. Signal Process. (ICICS)*, 2011, pp. 1–5.

[41] F. A. Kondori, S. Yousefi, H. Li, S. Sonning, and S. Sonning, "3D head pose estimation using the Kinect," in *Proc. Int. Conf. Wireless Commun. Signal Process. (WCSP)*, 2011, pp. 1–4.

[42] K. Khoshelham and S. O. Elberink, "Accuracy and resolution of Kinect depth data for indoor mapping applications," *Sensors*, vol. 12, no. 2, pp. 1437–1454, Feb. 2012.

[43] A. Oliver, S. Kang, B. C. Wünsche, and B. MacDonald, "Using the Kinect as a navigation sensor for mobile robotics," in *Proc. 27th Conf. Image Vis. Comput. New Zealand*, 2012, pp. 509–514.

[44] B. Vallet and B. Lévym, "Spectral geometry processing with manifold harmonics," *Comput. Graph. Forum*, vol. 27, no. 1, pp. 251–260, 2008.

[45] Y. Liu, B. Prabhakaran, and X. Guo, "Point-based manifold harmonics," *IEEE Trans. Vis. Comput. Graphics*, vol. 18, no. 10, pp. 1693–1703, Oct. 2012.

[46] M. Chuang, L. Luo, B. J. Brown, S. Rusinkiewicz, and M. Kazhdan, "Estimating the Laplace-Beltrami operator by restricting 3D functions," in *Proc. Symp. Geometry Process.*, vol. 28. 2009, pp. 1475–1484.

[47] D. Wang, S. Sun, X. Chen, and Z. Yu, "A 3D shape descriptor based on spherical harmonics through evolutionary optimization," *Neurocomputing*, vol. 194, pp. 183–191, Jun. 2016.

[48] M. Kazhdan, T. Funkhouser, and S. Rusinkiewicz, "Rotation invariant spherical harmonic representation of 3D shape descriptors," in *Proc. Symp. Geometry Process.*, vol. 6. 2003, pp. 156–164.

[49] R. Malladi, J. A. Sethian, and B. C. Vemuri, "Shape modeling with front propagation: A level set approach," *IEEE Trans. Pattern Anal. Mach. Intell.*, vol. 17, no. 2, pp. 158–175, Feb. 1995.

[50] W. E. Lorensen and H. E. Cline, "Marching cubes: A high resolution 3D surface construction algorithm," *ACM SIGGRAPH Comput. Graph.*, vol. 21, no. 4, pp. 163–169, 1987.

[51] S. Izadi *et al.*, "KinectFusion: Real-time 3D reconstruction and interaction using a moving depth camera," in *Proc. 24th Annu. ACM Symp. User Interface Softw. Technol.*, 2011, pp. 559–568.

[52] M. R. Jahanshahi, F. Jazizadeh, S. F. Masri, and B. Becerik-Gerber, "Unsupervised approach for autonomous pavement-defect detection and quantification using an inexpensive depth sensor," *J. Comput. Civil Eng.*, vol. 27, no. 6, pp. 743–754, 2013.

[53] W. R. Vavrik, L. D. Evans, J. A. Stefanski, and S. Sargand, "PCR evaluation–considering transition from manual to semi-automated pavement distress collection and analysis," Tech. Rep., 2013.

[54] P. J. Besl and N. D. McKay, "Method for registration of 3-D shapes," in *Proc. Int. Soc. Opt. Photon.*, 1992, pp. 586–606.

[55] B. Curless and M. Levoy, "A volumetric method for building complex models from range images," in *Proc. 23rd Annu. Conf. Comput. Graph. Interact. Techn.*, 1996, pp. 303–312.

[56] R. A. Newcombe *et al.*, "Kinectfusion: Real-time dense surface mapping and tracking," in *Proc. 10th IEEE Int. Symp. Mixed Augmented Reality (ISMAR)*, Oct. 2011, pp. 127–136.

[57] M. Desbrun, M. Meyer, P. Schröder, and A. H. Barr, "Discrete differential-geometry operators in nD," Caltech Multi-Res Model. Group, Tech. Rep., 2000.

[58] D.-T. Lee and B. J. Schachter, "Two algorithms for constructing a delaunay triangulation," *Int. J. Comput. Inf. Sci.*, vol. 9, no. 3, pp. 219–242, 1980.

Yuming Zhang received the M.S. degree in electrical engineering from the Institute of Electrical Engineering, Chinese Academy of Sciences, in 2002. He is currently pursuing the Ph.D. degree in computer engineering with The University of New Mexico (UNM), Albuquerque, NM, USA. He is currently a Research Assistant with the Department of Electrical and Computer Engineering, UNM. His research interests include physics-based animation/simulation, scientific visualization, image processing, transportation data analysis and visualization, large-scale traffic flow simulation, intelligent transportation systems and related topics.

Cong Chen received the Ph.D. degree in transportation engineering from The University of New Mexico in 2015. He is currently a Post-Doctoral Fellow with the Department of Civil and Environmental Engineering, University of Hawaii at Manoa. His research interests include traffic safety analysis and crash modeling, traffic operation and congestion pricing, GIS-based transportation infrastructure management, human factors in transportation systems, and intelligent transportation systems.

Dr. Chen serves as an Editorial Board Member of the Heighpubs *Journal of Civil and Environmental Engineering* and the *International Journal of Vehicular Telematics and Infotainment Systems*. He is a Member of the Predictive Methods Subcommittee for the Transportation Research Board (TRB) Highway Safety Performance Committee (ANB25) and the Research Needs Statements Subcommittee for the TRB Safety Data, Analysis, and Evaluation Committee (ANB20). He is also an invited referee for over 10 peer-reviewed journals and conferences. He was a recipient of the New Mexico Governors Exempt Fellowship and served as an Intern with the New Mexico Department of Transportation in 2014.

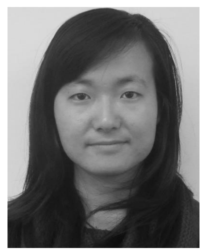

Qiong Wu received the B.S. degree in civil engineering from the Nanjing University of Aeronautics and Astronautics, Nanjing, China, in 2010, and the M.S. degree in highway and railway engineering from Tongji University, Shanghai, China, in 2012. After three years study in The University of New Mexico as a Ph.D. student, she transferred to the University of Hawaii at Manoa (UHM) to pursue her Ph.D. degree in 2016. Since 2016, she has been a Research Assistant with the Department of Civil and Environmental Engineering, UHM. Her research interests include traffic safety, intelligent transportation systems and autonomous vehicles.

Qi Lu was born in Huanggang, China, in 1982. He received the B.S. degree in computer science and technology from Hubei University, Wuhan, China, in 2006, and the M.S. degree in software system engineering from Aalborg University, Aalborg, Denmark, in 2011. He is currently pursuing the Ph.D. degree in computer science with The University of New Mexico, Albuquerque, NM, USA.

Su Zhang was born in Baoding, China, in 1983. He received the B.S. degree in construction management from China in 2006 and the M.S. degree in construction management from The University of New Mexico (UNM), Albuquerque, in 2010, where he is currently pursuing the Ph.D. degree in engineering with a focus of applying geospatial techniques for infrastructure management.

From 2008 to 2010, he was a Research Assistant with the Department of Civil Engineering, UNM. Since 2011, he has been a Research Assistant with the Department of Geography and Environmental Studies, UNM. His research interest includes geographic information sciences (GIS), remote sensing (RS), construction engineering and infrastructure management, application of GIS and RS in infrastructure management, and spatial analysis and modeling. He is an active member of the American Society of Civil Engineers, the American Society of Photogrammetry and Remote Sensing, and the New Mexico Geographic Information Council.

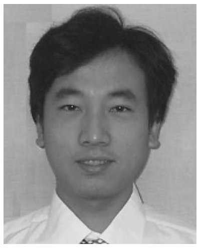

Guohui Zhang received the Ph.D. degree from the University of Washington (UW), Seattle, in 2000. He is currently an Assistant Professor with the Department of Civil and Environmental Engineering, University of Hawaii at Manoa, Honolulu. His research interests include transportation system operations and analysis, transportation data management and analysis, large-scale traffic simulation, geographic information system-based infrastructure asset management, and traffic detection systems.

Dr. Zhang serves as a Member of the Transportation Research Board Committee on Information Systems and Technology (ABJ50), the NCHRP Project Panel on Work Zone Capacity Methods for the Highway Capacity Manual (D03107), and the NCHRP Project Panel on Environmental Justice Analyses When Considering Toll Implementation or Rate Changes (D08100), and an Executive Board Member of the Chinese Overseas Transportation Association. He was a recipient of the Rising Star Award from the UW Smart Transportation Applications and Research Laboratory in 2008 and the Traffic Simulation Award from Planung Transport Verkehr AG in 2009.

Yin Yang received the Ph.D. degree in computer science from The University of Texas at Dallas in 2013. He is currently an Assistant Professor with the Department of Electrical Computer Engineering, The University of New Mexico, Albuquerque. His research interests include physics-based animation/simulation and related applications, scientific visualization, and medical imaging analysis.